Electronic transport across S_9 sulfur clusters

Jing-Xin Yu,[1] Xiang-Rong Chen,[1,2,*,†] and Stefano Sanvito[3,*,‡]
[1]*College of Physical Science and Technology, Sichuan University, Chengdu 610064, China*
[2]*International Centre for Materials Physics, Chinese Academy of Sciences, Shenyang 110016, China*
[3]*School of Physics and CRANN, Trinity College, Dublin 2, Ireland*
(Received 21 May 2010; revised manuscript received 13 July 2010; published 11 August 2010)

The transport properties of S_9 clusters sandwiched between gold electrodes are investigated with a combination of density-functional theory and the nonequilibrium Green's-function method. In general we find a rather large conductance both when the cluster is oriented with its symmetry axis parallel to the transport direction and when it is perpendicular to it. In both cases the transmission is dominated by several closely spaced and extremely broad cluster molecular orbitals so that the transmission coefficient is almost flat around the gold Fermi level. This is only marginally affected by the external bias so that the *I-V* characteristic remains almost linear at least up to 1 V and for both the orientations. Furthermore the electron transport is only little affected by the bond length between the cluster and the electrodes, with the largest sensitivity found for the perpendicular orientation. Our results are rationalized by analyzing the device density of states projected over the various molecular orbitals.

DOI: 10.1103/PhysRevB.82.085415 PACS number(s): 71.15.Mb

I. INTRODUCTION

Quantum transport across atomic-scaled conductors has recently received great attention since molecules may become building blocks for future logic devices and sensors.[1,2] In response to the experimental effort the last few years have also witnessed a substantial progress in developing materials-specific theories for electronic transport at the nanoscale.[3–9] Among the possible molecules used to make devices, small clusters have been intensively investigated[10–16] and studies have emerged about semiconductor,[10–13] transition metal either magnetic[14] or not,[15] and alkaline-earth metal clusters,[16] just to name a few. Also of interest is the transport across molecular objects, whose internal degrees of freedom can be manipulated electrically[17] since these can form electrically accessible molecular switches. As far as we know, there are to date no investigations over the electrical transport properties of nonmetallic clusters. This is the aim of our work.

In a conventional molecular device one wishes to attach the molecule of interest to the electrodes in a controlled way. This is because the typical electrical response depends not only on the intrinsic characteristics of the molecule itself but also and often more importantly on the interaction with the electrodes, its binding structure and bonding properties.[18,19] Currently the most common materials combination comprises gold electrodes and organic molecules anchored via the S atom of a thiol group.[20–24] This has the advantage that usually the S-Au bond is strong but also the drawback that the Au surface may be thermally unstable.[23,24] An additional disadvantage is that as thiol bonds to Au it looses any useful subsequent chemistry so that little further chemical manipulation is possible. Thus we find natural to look at all sulfur clusters, which naturally bond to Au but still preserve a rich chemical activity.

Recently, we have investigated the structures of sulfur clusters S_n $(2 \leq < n \leq 9)$ by using a finite-difference pseudopotential real-space density-functional theory (DFT) scheme combined with a Langevin molecular-dynamics annealing technique.[25,26] Here we focus on the $n=9$ sulfur cluster, S_9, which can be prepared in microcrystalline form[27–30] and can be found naturally in biological systems.[31] We report a first-principles investigation on the electrical response of S_9 sandwiched between semi-infinite gold electrodes with (100) orientation. The remaining of the paper is organized as follows: in Sec. II, we briefly describe the theoretical method and we provide some calculation details. Then, we present our results and the associated discussion. Finally, we summarize the paper and draw some conclusions.

II. THEORETICAL METHOD AND CALCULATION DETAILS

Our computational scheme combines DFT (Ref. 32) and the nonequilibrium Green's-function (NEGF) method[33,34] to calculate the electronic structure and the transport properties of two-terminal devices. In particular, we use the SMEAGOL code,[9,35,36] which implements the NEGF formalism for the single-particle Kohn-Sham Hamiltonian obtained from DFT calculations performed with SIESTA.[37] SMEAGOL is capable of the fully self-consistently modeling of the electrical properties of two-terminal devices formed by an atomic-scale object attached to two semi-infinite current/voltage electrodes. In brief, it is based on the standard three-region partition of the device of interest: a left-hand (L) and a right-hand side (R) current/voltage electrode (leads) and a central extended molecule (EM), which includes a few atomic layers of the leads.

The Green's function of the entire system is defined by direct inversion

$$(\varepsilon^{\dagger} S - H) G^{R}(E) = I, \tag{1}$$

where H is the Hamiltonian matrix, S is the overlap matrix, I is the infinitely dimensional identity matrix, $\varepsilon^{\dagger} = \lim_{\delta \to 0} + E + i\delta$, and E is the energy (note that here we assume the electronic structure to be expended over a local-orbital basis set,

 ©2010 The American Physical Society

as done in SIESTA and SMEAGOL). Unfortunately this is an infinite-dimensional object that cannot be calculated directly. However, owning the fact that the electrodes are good metals and they actively screen the perturbation introduced by the molecule, all the information concerning the scattering properties can be extracted solely from the retarded Green's function for the extend molecule, G_M^R, which is defined as

$$G_M^R(E) = \left[\varepsilon^+ S_M - H_M - \sum_L^R (E) - \sum_R^R (E) \right]^{-1}, \quad (2)$$

where the retarded self-energies for the left- and right-hand side leads are

$$\sum_L^R (E) = (\varepsilon^+ S_{ML} - H_{ML}) G_L^{0R}(E) (\varepsilon^+ S_{LM} - H_{LM}),$$

$$\sum_R^R (E) = (\varepsilon^+ S_{MR} - H_{MR}) G_R^{0R}(E) (\varepsilon^+ S_{RM} - H_{RM}). \quad (3)$$

Here G_L^{0R} and G_R^{0R} are the retarded surface Green's function of the leads.[36,38] The Green's function in Eq. (2) is a matrix with finite dimension and the conductance associated to the two-probe device can be calculated by using the Fisher-Lee's relation[34,39]

$$G = \frac{2e^2}{h} \mathrm{Tr}[\Gamma_L G_M^{R+} \Gamma_R G_M^R], \quad (4)$$

where

$$\Gamma_\alpha(E) = i \left[\sum_\alpha^R (E) - \sum_\alpha^R (E)^+ \right]. \quad (5)$$

Finally the two-terminal current, I, can be calculated by integrating the conductance over the bias window

$$I = \frac{e}{h} \int dE \, \mathrm{Tr}[\Gamma_L G_M^{R+} \Gamma_R G_M^R][f(E-\mu_L) - f(E-\mu_R)]. \quad (6)$$

Note that when an external electrical potential (bias voltage) is applied, the conductance entering in Eq. (6) should be calculated by iterating self-consistently the Green's function of Eq. (2) together with an equation providing the single-particle Hamiltonian of the EM (the Kohn-Sham Hamiltonian in this case). More calculation details on how this procedure is performed in SMEAGOL can be found in the literature.[35,36]

Our DFT calculations use the Perdew-Zunger form[40] of the local-density approximation to the exchange-correlation functional. We use respectively a double-zeta basis set for the S atom and the single-zeta basis set for the gold atoms in the electrodes.[20] The scalar-relativistic Troullier-Martins pseudopotentials[41] in nonlocal form generated from the $5d^{10}6s^1$ reference configuration for gold atom and $3s^2 3p^4$ for sulfur atom were employed, respectively. The periodic boundary conditions are applied in the basal plane (orthogonal to the transport direction) with four irreducible k points in the two-dimensional Brillouin zone. A k-grid sampling of $2 \times 2 \times 100$ for the gold electrodes was employed, together with a mesh cutoff of 200 Ry. The same mesh cutoff is used also in the self-consistent transport calculations. We consider 100 real and 50 complex energy points when integrating the Green's function.

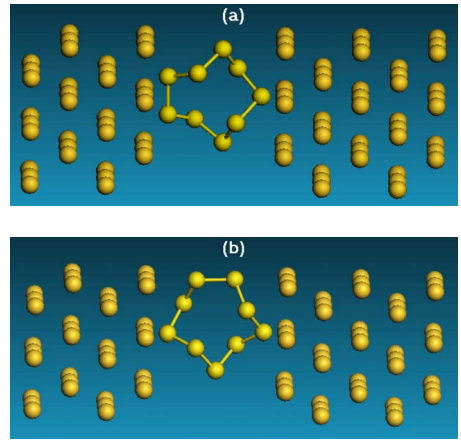

FIG. 1. (Color online) Atomic configuration of the two devices investigated in this work comprising an S_9 cluster and gold electrodes. In (a) the symmetry axis of S_9 is parallel to the direction of transport (PAC) and in (b) it is perpendicular (PPC) (color code: Au yellow and S bright yellow).

III. RESULTS AND DISCUSSION

The device geometries investigated in this work are presented in Fig. 1. In both cases the EM, in addition to S_9, includes four and five Au atomic layers, respectively, to the left- and right-hand sides of the cluster. These have the same crystal structure of the leads and they are sufficient to screen the perturbation that the S_9 cluster has over the electrodes' electronic structure.[9] We consider two orientations of S_9 with respect to the electrodes. In the first [Fig. 1(a)] the symmetry axis of S_9 is parallel to the transport direction (parallel configuration—PAC). The anchoring structure has two S atoms at the Au (100) hollow site positions on one side while a single S is placed at atop position at the other side. In contrast, the S_9 symmetry axis of the second configuration [Fig. 1(b)] is perpendicular to the direction of transport (Per-Pendicular configuration—PPC) and the binding S atoms are both placed at Au atop sites.

In both cases, the electrodes have an ideal fcc (100) structure with the lattice parameter of bulk gold. The equilibrium geometry of the S_9 cluster is taken from our previous work[26] while the geometry of the entire device is evaluated by performing total-energy calculations for different cluster to electrodes distances (without further relaxing the internal structure of the electrodes and of S_9). The optimization is performed by fixing the distance between the two electrodes and by moving rigidly the cluster along the direction perpendicular to the leads' surfaces (the position in the plane remains fixed). We found that the total energy is minimized for a symmetric position, i.e., when the distance between the cluster and the surface is identical for the two electrodes. This gives us an equilibrium distance of 2.4 Å for both the hollow and the atop site (see Fig. 2). Note however that in

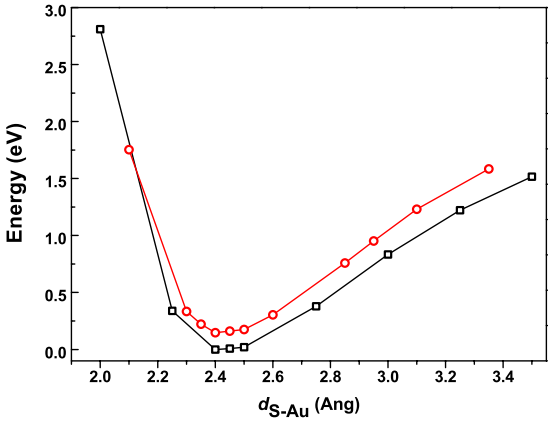

FIG. 2. (Color online) Total energy as a function of the distance, $d_{\text{S-Au(100)}}$, between the S_9 cluster and the electrodes for the PAC (black square) and the PPC (red circle). The zero points of the energy have been chosen with respect to the optimal structure of PAC.

the case of the hollow site the distance of 2.4 Å is that between the plane of the hollow site and S and it corresponds to an S-Au bond length of about 2.65 Å. Our simulations also confirm the intuitive idea that the device with the larger number of Au-S bonds is the most stable, as demonstrated by the fact that at the equilibrium position the PAC has a lower energy than the PPC.

Since the S_9 cluster is not a rigid object and it is well known that the presence of S in a molecular junction may introduce a substantial structural relaxation[42,43] we have performed additional geometry optimization of the S_9 cluster in the Au/S_9/Au device. We start the simulations with the cluster sitting at the previously calculated equilibrium positions for both the PAC and the PPC. Furthermore we relax by conjugate gradient only the S atoms and keep fixed to the bulk positions the Au. We find that the internal structure relaxation of S_9 is marginal in the PAC with the exception of a modest shift (0.07 Å) of the bonding site from atop to hollow. In contrast the PPC relaxes much more. In particular, we observe that the S_9 symmetry axis rotates toward the transport direction. The final optimized geometry is extremely similar to the PAC, corroborating our previous conclusion based on total-energy considerations about the stabilities of the two geometries. This essentially means that there is only one stable bonding configuration. Still in order to study the effect of bonding over the transport we have carried out calculations also for the original (unrelaxed) PPC.

In Fig. 3, we display the transmission coefficients as a function of energy at zero bias, $T(E;V)$, and the I-V characteristics of both the geometrical configurations. As one can easily see there are no important differences between the two geometries and in general $T(E;V)$ appears always rather smooth with energy. In particular, the transmission at around the Au Fermi level (E_F) is characterized by a multiplet of closely spaced peaks, corresponding to characteristic molecular orbitals, that spreads over about 1 eV. These states however are quite broad because of the strong electronic interaction of S_9 with the electrodes so that the resulting transmission coefficient is almost featureless. Going into more

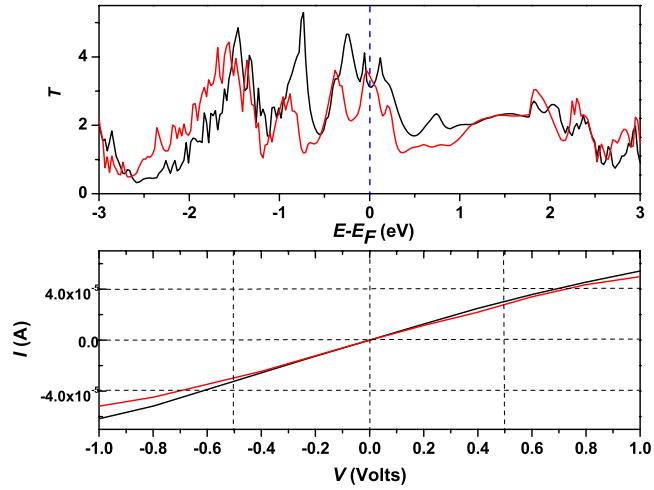

FIG. 3. (Color online) Transport properties of an S_9 cluster attached to gold (100) electrodes. In the top panels we present the transmission coefficients as a function of energy at zero bias, $T(E;V)$, while in the lower ones the I-V curves. Black line is for the PAC and red line for the PPC. The blue dashed vertical line mark the zero-bias windows.

details the only appreciable change in going from the PAC to the PPC is the exact position of E_F with respect to the multiplet. In fact in the case of the PAC the Au Fermi energy is placed in between two transmission peaks while it is actually pinned at one peak in the PPC. The conductance at zero bias (i.e., the conductance in the linear-response limit) reflects this difference and it is $3.04G_0$ ($G_0=2e^2/h$) for PAC and $3.5G_0$ for PPC. There is also a second minor difference that distinguishes the two configurations, namely, that the width of the highest occupied molecular orbital (HOMO) transmission peaks in the PAC is narrower than that of the PPC. This is attributed to the different Au-S bond length of the hollow and atop sites, although a fully quantitative assessment[14,44] is difficult in this case since $T(E)$ here is rather too smooth.

In general and for both the geometries this is quite modest with little modifications as the electric field is increases and as expected in a strong electronic coupling situation. For both the PAC and PPC there are almost no changes in the shape and amplitude of $T(E;V)$ with V, except for a some minor rearrangement of the peak structure at around E_F. Therefore the only effect of the bias is that of including more spectral range in the integral giving the current [see Eq. (6)]. As a consequence the I-V shows a monotonic behavior with a rather constant slope. Finally in both the PAC and PPC the I-V's appear rather symmetric, as a result of both the strong electronic coupling and, in the case of the PPC, of the symmetric device geometry.

The influence of the S_9 bonding to the electrodes over the transport properties is investigated, where we compare the zero bias $T(E)$ for different distances between the terminal S atoms and the Au surface, $d_{\text{S-Au(100)}}$. Again the variations are rather small, both when the junctions are compressed ($d_{\text{S-Au(100)}}<2.4$ Å) and when they are stretched ($d_{\text{S-Au(100)}}>2.4$ Å). In general an elongation of the Au-S bond reduces the electronic coupling between the cluster and the electrodes and produces a sharpening of the transmission peak.

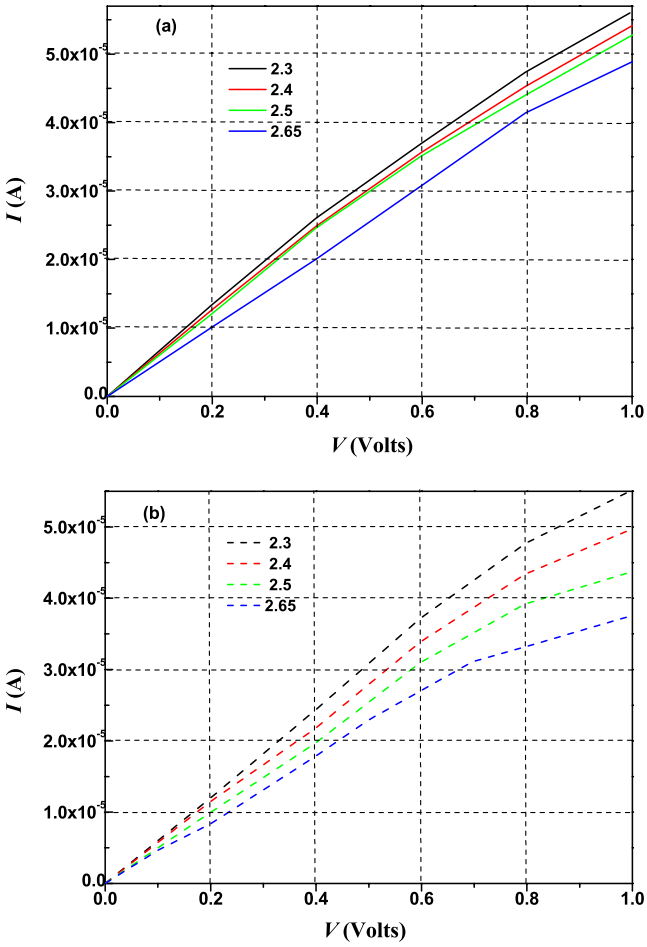

FIG. 4. (Color online) *I-V* curves calculated for different distances between the S_9 cluster and the electrodes, $d_{\text{S-Au(100)}}$: (a) PAC and (b) PPC.

Compression has the opposite effect and $T(E)$ becomes even smoother than at equilibrium. Interestingly for both the PAC and the PPC the relative position of the peak multiplet responsible for the transport and E_F remains essentially unchanged under both bond compression and elongation within the range investigated here. This means that E_F is kept in between two transmission peaks for PAC while it stays pinned at one of them for the PPC. This is essentially due to a small realignment of the HOMO of the molecule to E_F of gold, which counterbalances a reduction in width of the associated transmission peak. Such a dynamics is driven by the dependence of the charge transfer between the molecule and the metal as a function of $d_{\text{S-Au(100)}}$ and it has been previously reported for the S-Au bond of the thiol group in organic molecules anchored to Au at undercoordinated sites.[21] Certainly upon further increase in $d_{\text{S-Au(100)}}$ one expects the transmission to eventually be suppressed and the transmission coefficient to became smaller. Finally it is worth noticing that the peak structure of $T(E)$ around E_F for long bond distances ($d_{\text{S-Au(100)}}=2.65$ Å) is sharper for the PPC then for the PAC indicating that the atop site is more sensitive to changes that the hollow position.

The different *I-V* characteristics of the system calculated at different $d_{\text{S-Au(100)}}$ are reported in Fig. 4. In the low-bias region and for the PAC the conductances are calculated to be $3.3G_0$, $3.04G_0$, $3.25G_0$, and $2.58G_0$, respectively, for $d_{\text{S-Au(100)}}$ 2.3 Å, 2.4 Å, 2.5 Å, and 2.65 Å. The PPC also presents a similar situation. Here there we find low-bias conductances of $3.0G_0$, $3.5G_0$, $3.1G_0$, and $2.3G_0$, respectively, for $d_{\text{S-Au(100)}}$ of 2.3 Å, 2.4 Å, 2.5 Å, and 2.65 Å. Apart from these quantitative differences, then the various *I-V*'s look rather similar to each other. We note that the *I-V* of the PAC is less sensitive to bond-length changes than that of PPC. For this latter we observe that as the bond distance increases there is a gradual development of a two-slope feature in the *I-V*. For instance, for $d_{\text{S-Au(100)}}=2.65$ Å there is a change in conductance at around 0.75 V. This reflects the more sharp transmission peak structure of the PPC at large bond distances.

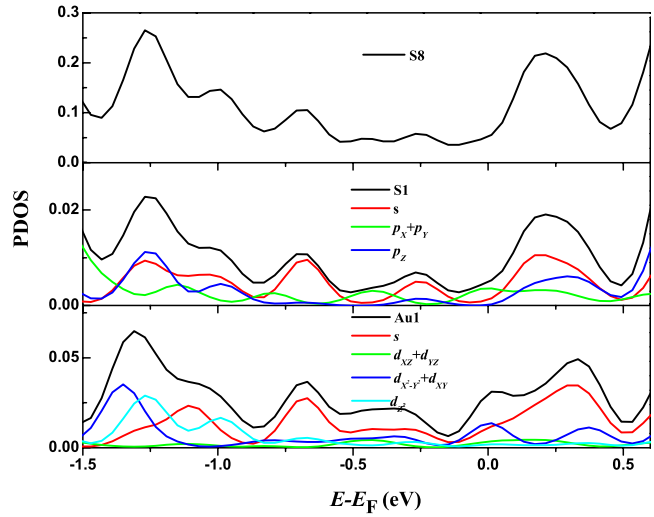

FIG. 5. (Color online) DOS projected over the sulfur atoms of the S_9 cluster and the Au atom corresponding to the adatom position for PAC. The middle panels are for the S atom adjacent to the adatom while the top ones are for the remaining S in the cluster.

The influence of the electronic structure on the transport properties can be investigated by analyzing the projected density of states (PDOS) over the various atomic orbitals around the Au Fermi energy (see Fig. 5). In Fig. 5, we plot the PDOS of the Au and S atoms bonded at the atop position and that of the remaining eight S for the PAC. We note that there is an expected one-to-one mapping between the S DOS and the position of the transmission peaks for the two devices. In particular, we observe that the Au Fermi level is placed in between a large peak in the DOS mostly originating from S atoms and a smaller one, which receives equal contribution from S and Au. This confirms our previous attribution of the current due to the interpeak energy region between the HOMO and the lowest unoccupied molecular orbital for the PAC. A similar analysis can be carried out for the PPC confirming the HOMO conductance at low bias. Going into more details about the orbital content of the DOS we note that for both PAC and PPC most of the S-related DOS around E_F originates from the *s* orbitals, with some smaller contributions from p_x and p_y (here the *z* axis is along the transport direction while the *x-y* plane is orthogonal to it). Likewise for Au the *s* orbital dominates the DOS al-

though contributions from $d_{x2}-d_{y2}$ and d_{xy} account for a part of it especially near the Fermi level.

IV. CONCLUSIONS

We have presented the DFT-NEGF electron-transport calculations for S_9 clusters attached to Au (100) electrodes. In particular, we have considered two geometrical configurations in which the S_9 is attached to the electrodes with its symmetry axis either parallel or perpendicular to the transport direction. It is found that the transmission coefficient in the spectral window relevant for the current up to about 1 V is characterized by several closely spaced and extremely broad cluster molecular orbitals so that the transmission coefficient is almost flat around the gold Fermi level. This yields rather linear *I-V* curves for both the device configurations. Interestingly the bond distance between S_9 and the electrodes affects little this picture and the *I-V*'s are predicted rather stable with geometrical changes. In this respect the PPC is more sensitive because of the double adatom anchoring geometry.

ACKNOWLEDGMENTS

The authors would like to thank the support by the National Natural Science Foundation of China under Grant No. 10776022 and by the SRFDP under Grant No. 20090181110080. The SMEAGOL project (S.S.) is sponsored by Science Foundation of Ireland and CRANN.

*Corresponding author.
†x.r.chen@tom.com
‡sanvitos@tcd.ie

[1] L. Venkataraman, J. E. Klare, C. Nuckolls, M. S. Hybertsen, and M. L. Steigerwald, Nature (London) **442**, 904 (2006).
[2] J. R. Heath and M. A. Ratner, Phys. Today **56**(5), 43 (2003).
[3] E. G. Emberly and G. Kirczenow, Phys. Rev. B **58**, 10911 (1998).
[4] J. G. Kushmerick, D. B. Holt, J. C. Yang, J. Naciri, M. H. Moore, and R. Shashidhar, Phys. Rev. Lett. **89**, 086802 (2002).
[5] M. Di Ventra, S. T. Pantelides, and N. D. Lang, Phys. Rev. Lett. **84**, 979 (2000).
[6] E. G. Emberly and G. Kirczenow, Phys. Rev. Lett. **87**, 269701 (2001).
[7] J. Heurich, J. C. Cuevas, W. Wenzel, and G. Schon, Phys. Rev. Lett. **88**, 256803 (2002).
[8] R. Stadler, K. S. Thygesen, and K. W. Jacobsen, Nanotechnology **16**, S155 (2005).
[9] A. R. Rocha, V. M. Garcia-Suarez, S. Bailey, C. Lambert, J. Ferrer, and S. Sanvito, Nature Mater. **4**, 335 (2005).
[10] C. Roland, V. Meunier, B. Larade, and H. Guo, Phys. Rev. B **66**, 035332 (2002).
[11] Z. X. Dai, X. H. Zheng, X. Q. Shi, and Z. Zeng, Phys. Rev. B **72**, 205408 (2005).
[12] Z. X. Dai, X. Q. Shi, X. H. Zheng, and Z. Zeng, Phys. Rev. B **73**, 045411 (2006).
[13] Z. X. Dai, X. Q. Shi, X. H. Zheng, X. L. Wang, and Z. Zeng, Phys. Rev. B **75**, 155402 (2007).
[14] C. D. Pemmaraju, I. Rungger, and S. Sanvito, Phys. Rev. B **80**, 104422 (2009).
[15] C. Cao, A. F. Kemper, L. Agapito, J.-W. Zhang, Y. He, A. Rinzler, H.-P. Cheng, X.-G. Zhang, A. R. Rocha, and S. Sanvito, Phys. Rev. B **79**, 075127 (2009).
[16] R. Gutiérrez, F. Grossmann, O. Knospe, and R. Schmidt, Phys. Rev. A **64**, 013202 (2001).
[17] N. Baadji, M. Piacenza, T. Tugsuz, F. Della Sala, G. Maruccio, and S. Sanvito, Nature Mater. **8**, 813 (2009).
[18] H. Basch, R. Cohen, and M. A. Ratner, Nano Lett. **5**, 1668 (2005).
[19] Y. Xue and M. A. Ratner, Phys. Rev. B **69**, 085403 (2004).
[20] R. X. Zhang, G. H. Ma, R. Li, Z. K. Qian, Z. Y. Shen, X. Y. Zhao, S. M. Hou, and S. Sanvito, J. Phys.: Condens. Matter **21**, 335301 (2009).
[21] C. Toher and S. Sanvito, Phys. Rev. B **77**, 155402 (2008).
[22] S. Martín, D. Zsolt Manrique, V. M. García-Suárez, W. Haiss, S. J. Higgins, C. J. Lambert, and R. J. Nichols, Nanotechnology **20**, 125203 (2009).
[23] G. S. Tulevski, M. B. Myers, M. S. Hybertsen, M. L. Steigerwald, and C. Nuckolls, Science **309**, 591 (2005).
[24] C. Toher and S. Sanvito, Phys. Rev. Lett. **99**, 056801 (2007).
[25] Y. L. Bai, X. R. Chen, X. D. Yang, and X. L. Zhou, J. Phys. B **36**, 4511 (2003).
[26] J. Q. Lan, X. R. Chen, Y. L. Bai, and J. Zhu, Physica B **405**, 148 (2010).
[27] R. Steudel, in *Studies in Inorganic Chemistry*, edited by A. Muller and B. Krebs (Elsevier, Amsterdam, 1984), Vol. 5.
[28] D. Hohl, R. O. Jones, R. Car, and M. Parrinello, J. Chem. Phys. **89**, 6823 (1988).
[29] R. Steudel, Nova Acta Leopold. **59**, 231 (1985).
[30] R. Steudel, T. Sandow, and J. Steidel, Z. Naturforsch., Part B **40**, 594 (1985).
[31] R. Steudel, G. Hpldt, T. Gobel, and W. Hazeu, Angew. Chem. **99**, 143 (1987).
[32] W. Kohn and L. Sham, Phys. Rev. **140**, A1133 (1965).
[33] L. P. Kadanoff and G. Baym, *Quantum Statistical Mechanics Benjamin/Cummings* (Benjamin, New York, 1962).
[34] S. Datta, *Electronic Transport in Mesoscopic System* (Cambridge University Press, Cambridge, 1995).
[35] A. R. Rocha, V. M. Garcia-Suarez, S. Bailey, C. Lambert, J. Ferrer, and S. Sanvito, Phys. Rev. B **73**, 085414 (2006).
[36] I. Rungger and S. Sanvito, Phys. Rev. B **78**, 035407 (2008).
[37] J. M. Soler, E. Artacho, J. D. Gale, A. Garcia, J. Junquera, P. Ordejon, and D. Sanchez-Portal, J. Phys.: Condens. Matter **14**, 2745 (2002).
[38] S. Sanvito, C. J. Lambert, J. H. Jefferson, and A. M. Bratkovsky, Phys. Rev. B **59**, 11936 (1999).

[39] D. S. Fisher and P. A. Lee, Phys. Rev. B **23**, 6851 (1981).
[40] J. P. Perdew, Phys. Rev. B **33**, 8822 (1986).
[41] N. Troullier and J. L. Martins, Phys. Rev. B **43**, 1993 (1991).
[42] I. S. Kristensen, D. J. Mowbray, and K. S. Thygesen, J. Phys.: Condens. Matter **20**, 374101 (2008).
[43] M. Strange, O. Lopez-Acevedo, and H. Häkkinen, J. Phys. Chem. Lett. **1**, 1528 (2010).
[44] R. Stadler, J. Phys.: Conf. Ser. **61**, 1097 (2007).